

# Drop pinch-off and filament dynamics of wormlike micellar fluids

Linda B. Smolka<sup>1</sup>, Andrew Belmonte\*

*The W.G. Pritchard Laboratories, Department of Mathematics, Pennsylvania State University,  
University Park, PA 16802, USA*

Received 23 May 2001 ; received in revised form 29 October 2002

---

## Abstract

Observations are presented of several novel phenomena involved in the dynamics of a pendant drop of viscoelastic micellar fluid falling through air. Generally, when a drop falls a filament forms connecting it to the orifice; the filament eventually breaks due to an instability. The filament dynamics and instabilities reported here are very different from the standard Newtonian and non-Newtonian cases. At low surfactant concentration, the cylindrical filament necks down and pinches off rapidly ( $\sim 10$  ms) at one location along the filament. After pinch-off, the free filament ends retract and no satellite drops are produced. At higher concentrations, the pinch-off also occurs along the filament, but in a more gradual process ( $\sim 1$  s). Furthermore, the free filament ends do not fully retract, instead retaining some of their deformation. The falling drop is also observed to slow or even stop (stall) before pinch-off, indicating that sufficient elastic stress has built up to balance its weight. We investigate this stall by generalizing Keiller's simple model for filament motion [J. Non-Newtonian Fluid Mech. 42 (1992) 37], using instead the FENE-CR constitutive equation. Numerical simulations of this model indicate that stall occurs in the range of low solvent viscosity, high elasticity, and high molecular weight. At the highest concentrations, we observe a surface "blistering" instability along the filament long before pinch-off occurs.

© 2003 Elsevier B.V. All rights reserved.

*Keywords:* Liquid drops; Liquid filament; Extensional flow; Pinch-off; Wormlike micelles; Viscoelasticity; FENE-CR model; Surface instability

---

## 1. Introduction

Viscoelastic fluids composed of weakly interacting molecular aggregates in solution have recently been shown to exhibit several new dynamical phenomena not seen in the more standard non-Newtonian fluids such as polymer solutions or melts. These fluids include wormlike micellar solutions [2], complex lamellar phases [3,4], clay suspensions [5], or associating polymer solutions [6]. For instance, in Saffman–Taylor fingering experiments with associating polymers, a striking transition from viscous fingering to solid-like

---

\* Corresponding author.

*E-mail address:* belmonte@math.psu.edu (A. Belmonte).

<sup>1</sup> Present address: Department of Mathematics, Duke University, Box 90320, Durham, NC 27708, USA.

fracture is observed [7,8]. In the flow of wormlike micellar solutions, there is increasing experimental evidence of intrinsic oscillations, including measurements under an imposed steady shear rate [9], the repeated growth and tearing of small structures in a Couette cell [10], oscillating rings in a constant stress parallel plate rheometer [11,12], and the non-transient jumping of a rising bubble [13] or sedimenting sphere [14]. Although the cause of these oscillations is not understood, it may be due to shear-driven transitions to different microscopic states [15–18].

The pinch-off of a pendant drop of Newtonian fluid in air is a well-known phenomenon involving a topological change from a drop attached to an orifice to a freely falling droplet—see [19] for an extensive review. For most fluids, when the weight of a pendant drop exceeds the surface tension force holding it to the orifice, the drop begins to fall. During this process a filament is typically drawn out connecting the drop to the orifice. This filament eventually becomes unstable to a capillary instability which leads to pinch-off of the drop [20–22]. It is well-known that these dynamics can be vastly different for polymer fluids, where viscoelastic effects can delay the breakup of the filament [23] despite the presence of large “bead-on-string” type perturbations [24,25].

In this paper, we report experimental observations of new dynamics for drops composed of viscoelastic surfactant solutions, the so-called “wormlike” micellar fluids [2], falling through air. For low concentrations we observe a localized filament failure that is both liquid-like and solid-like in its behavior, producing no satellite drops. At higher concentrations, we find evidence of an extensionally driven gel transition based on surface blistering along the interface and an incomplete recovery of the stretched filament after pinch-off. We have also observed that the drop can stop in its downward motion for as long as 1 s. This observation is qualitatively reproduced in a simple model utilizing the FENE-CR constitutive equation [26]; our model is a generalization of one proposed by Keiller [1]. This work addresses the forces which slow down the drop, and the dependence of this process on the parameters in the model. Although this model is not specific to micellar solutions, the range of parameters in which the drop stops, that of low solvent viscosity and high elasticity, is a characteristic of wormlike micellar fluids.

## 2. Experimental setup

The experimental apparatus, which has been described previously [21,22], consists of a plastic (Lucite) reservoir, a digital imaging camera and processor. The fluid flowed under gravity from the reservoir, which was open to the atmosphere, through a needle valve which controlled the flow rate, and finally through a lower tube of length 6.6 cm with inner radius 1.54 mm. In all of the experiments, the period of the drops was about 30 s per drop. The apparatus was set on a Newport vibration isolated table, and enclosed in a Lucite box to reduce air currents. Images and video sequences of the drops were obtained using a Kodak Ektapro 1012 EM Motion Analyzer [21,22]. All of the experiments were performed at room temperature, which ranged from 20 to 23 °C.

The experimental fluids are aqueous solutions of the wormlike micellar system cetyltrimethylammonium bromide (CTAB)/sodium salicylate (NaSal) [15,27,28], or cetylpyridinium chloride (CPCl)/NaSal [17,28,29]. These are two examples of several aqueous solutions involving the organic salt NaSal, which facilitates the formation of long tubular “wormlike” micelles of cationic surfactants [28]. These tubes have diameter  $\sim 10$  nm [30], and can be as long as 1  $\mu\text{m}$  [31]. In these solutions, the micelles break and reform reversibly [16], thus the “molecular weight” distribution is a kinetic balance which can be affected by the flow. In fact, shear can cause the formation of large-scale structures [10,18] that strongly align in

the direction of the flow [28,32]. These structures are much larger than individual micellar tubes with lengths in excess of 100  $\mu\text{m}$  and diameters in the range of 0.2–1  $\mu\text{m}$  [10].

The CTAB, CPCI, and NaSal used here are obtained from Aldrich, and dissolved in distilled deionized water without further purification. The fluids are mixed for several days, then allowed to sit for a day before use. We focus on three different solutions that display qualitatively different behavior during pinch-off: a 6 mM equimolar solution of CTAB/NaSal which is the most liquid-like, a more elastic solution of 80 mM CPCI and 60 mM NaSal, and a very elastic solution of 100 mM CPCI and 60 mM NaSal. Two of these systems are among the most studied systems rheologically: equimolar CTAB/NaSal is one of the first systems studied [15,27,30], while 100 mM CPCI/60 mM NaSal is a standard recipe studied in detail by Rehage and Hoffman [28] and Grand et al. [29] among others. However, the shear rheology of wormlike micellar fluids can be problematic due to apparent inhomogeneities in cone and plate [11,33] and Couette rheometers [10]. For equimolar CTAB/NaSal solutions at 23  $^{\circ}\text{C}$ , concentrations of 5.0 and 7.5 mM are known to be shear thinning, with a measured zero shear viscosity  $\eta_0$  between 0.4 and 1.0 P [34] (some variation is due to cone angle). The measured relaxation times  $\lambda$  are less than 0.1 s [34], from which we can estimate an elastic modulus of  $G \simeq \eta_0/\lambda = 10 \text{ dyn/cm}^2$ . For 100 mM CPCI/60 mM NaSal, shear thinning has also been observed [28,29], with measured values at 23.5  $^{\circ}\text{C}$  of  $\lambda \simeq 2.5 \text{ s}$  and  $G \simeq 270 \text{ dyn/cm}^2$  [29] (which gives  $\eta_0 \simeq \lambda G = 675 \text{ P}$ ).

Because our third fluid is not commonly studied, we report its viscoelastic fluid properties here. Rheological measurements of the 80 mM CPCI/60 mM NaSal solution were performed with a temperature controlled Rheometrics RFS-III rheometer, in strain controlled mode. The fluid was tested in a standard Couette cell at  $T = 22.8 \pm 0.4 \text{ }^{\circ}\text{C}$ , with an inner cylinder of diameter 32 mm and height 33 mm, and a gap of 1 mm. Steady state shear stress measurements show that this fluid is shear thinning, similar to the other two fluids discussed above. The shear stress  $\sigma_{12}$  is plotted as a function of applied shear rate  $\dot{\gamma}$  in Fig. 1, where we note that a stress plateau is observed, a well-known characteristic of wormlike micellar fluids [16,28,29]. The apparent shear viscosity  $\eta_a \equiv \sigma_{12}/\dot{\gamma}$  was calculated from the data in Fig. 1. From this, we find that the zero shear viscosity  $\eta_0 \simeq 430 \text{ P}$ , and estimate the relaxation time (where  $\eta_a$  thins below  $\eta_0$ ) as  $\lambda \simeq 1.4\text{--}2.5 \text{ s}$ .

The linear viscoelastic properties were also determined for this fluid using the Couette geometry. The dynamic storage modulus  $G'$  and loss modulus  $G''$  for 15% strain are shown as a function of frequency  $\omega$  in Fig. 2(a). The intersection of  $G'$  and  $G''$  gives another estimate of the relaxation time,  $\lambda \simeq 1.7 \text{ s}$ . At low frequencies, the moduli show the “liquid-like” scalings  $G'' \sim \omega$  and  $G' \sim \omega^2$  [2]. The overall shape of these curves is close to a single relaxation time Maxwell model [2], best seen in a Cole–Cole representation plotting  $G''$  versus  $G'$ , as shown in Fig. 2(b). For a Maxwell fluid this curve should fall on a semicircle of radius  $G/2$ , where  $G$  is the constant elastic modulus of the fluid:

$$(G'(\omega) - \frac{1}{2}G)^2 + G''(\omega)^2 = (\frac{1}{2}G)^2. \quad (1)$$

While there is a clear deviation from this functional dependence at higher frequencies, also seen in similar systems [17,35], the best fit semicircle (the solid curve in Fig. 2(b)) gives  $G = 220 \text{ dyn/cm}^2$ .

In extensional flows, wormlike micelles are known to strongly align with streamlines in the flow [36], thus one would expect the extensional viscosity of the fluid to be relevant to the flow dynamics. Although extensional rheometry of complex fluids is notoriously difficult to measure, there are a few studies for wormlike micellar solutions [36–38]. These studies reveal that the extensional viscosity for some micellar solutions can vary with gradients in the flow. In particular, these solutions elongationally thicken for stretch rates greater than the reciprocal of the fluid relaxation time. This behavior is similar to

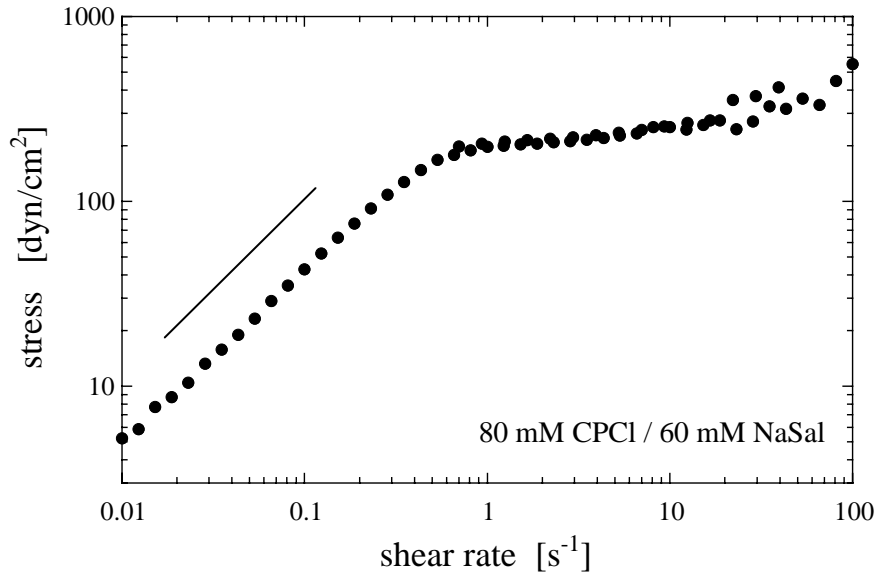


Fig. 1. Steady rheology of 80 mM CPCl/60 mM NaSal at  $T = 22.8^\circ\text{C}$ : stress vs. shear rate. The solid line corresponds to a Newtonian (linear) scaling.

the nonlinear dynamics displayed by polymer solutions. However, in contrast to polymer solutions, these micellar solutions attain a peak in their extensional viscosity at a critical stretch rate, then elongationally thin for higher stretch rates. Although this transition from elongational thickening to thinning is not well understood, it may be due to breaking or slipping of the micelles in the flow [36,37].

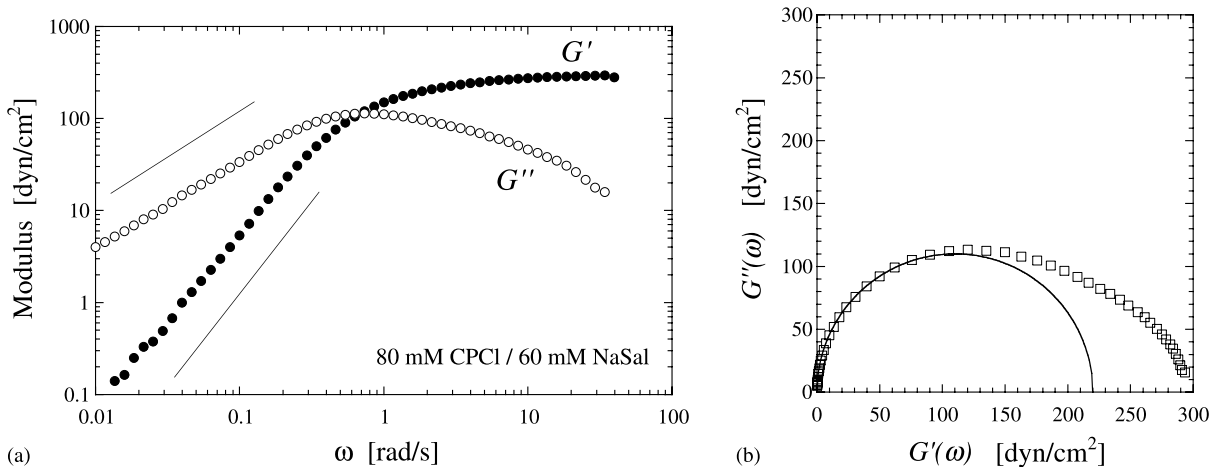


Fig. 2. Dynamic rheology of 80 mM CPCl/60 mM NaSal at  $T = 22.8^\circ\text{C}$ : (a) storage and loss moduli  $G'$  and  $G''$  as functions of frequency. The solid lines show the scalings  $G'' \sim \omega$  and  $G' \sim \omega^2$  (see text); (b) Cole–Cole plot of the same data, where the solid curve is the fitted semicircle with elastic modulus  $G = 220 \text{ dyn/cm}^2$  (see Eq. (1)).

### 3. Pinch-off and filament dynamics

For most fluids when the weight of a pendant drop exceeds the surface tension force holding it to the orifice, the drop begins to fall [19]. As the drop falls a filament forms connecting it to the orifice. Subsequently, the filament breaks in some way, and the drop separates from the orifice. We investigate the main features of this pinch-off process using high-speed digital imaging and compare the behavior for three aqueous micellar solutions.

#### 3.1. 6 mM CTAB/NaSal

Fig. 3 illustrates the main features of the filament instability for the 6 mM CTAB/NaSal solution. At this concentration the fall of the drop produces a very smooth and cylindrical filament, which subsequently pinches off at a single location along the filament. In this example, the filament in Fig. 3(a) is 6.5 cm long and has been smooth and cylindrical for over 3 s. In the next 18 ms, between frames (a) and (b), a perturbation appears approximately 2.2 cm from the orifice and the pinch-off occurs between frames (c) and (d). The full transition from a cylindrical filament to a detached droplet occurs over a comparatively short period of time (here, less than 40 ms). Surprisingly, the rest of the filament remains cylindrical during this entire process. The local nature of this breaking instability is analogous to the yield or failure of an elastic solid or the ductile failure in certain metals and alloys, and similar to the extensional rupture

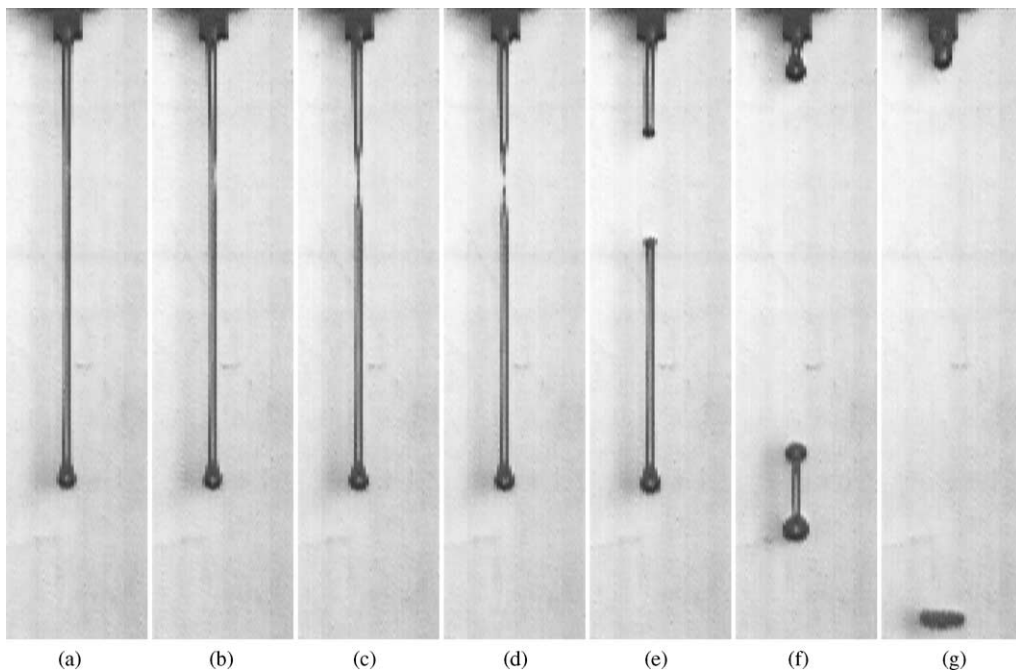


Fig. 3. The pinch-off of a falling drop of an aqueous solution of 6 mM CTAB/NaSal. The relative times of each image are (a) 0 ms, (b) 18 ms, (c) 35 ms, (d) 38 ms, (e) 47 ms, (f) 85 ms, and (g) 111 ms. The resolution is 0.45 mm per pixel. The size of each image is 2.7 cm  $\times$  10.1 cm.

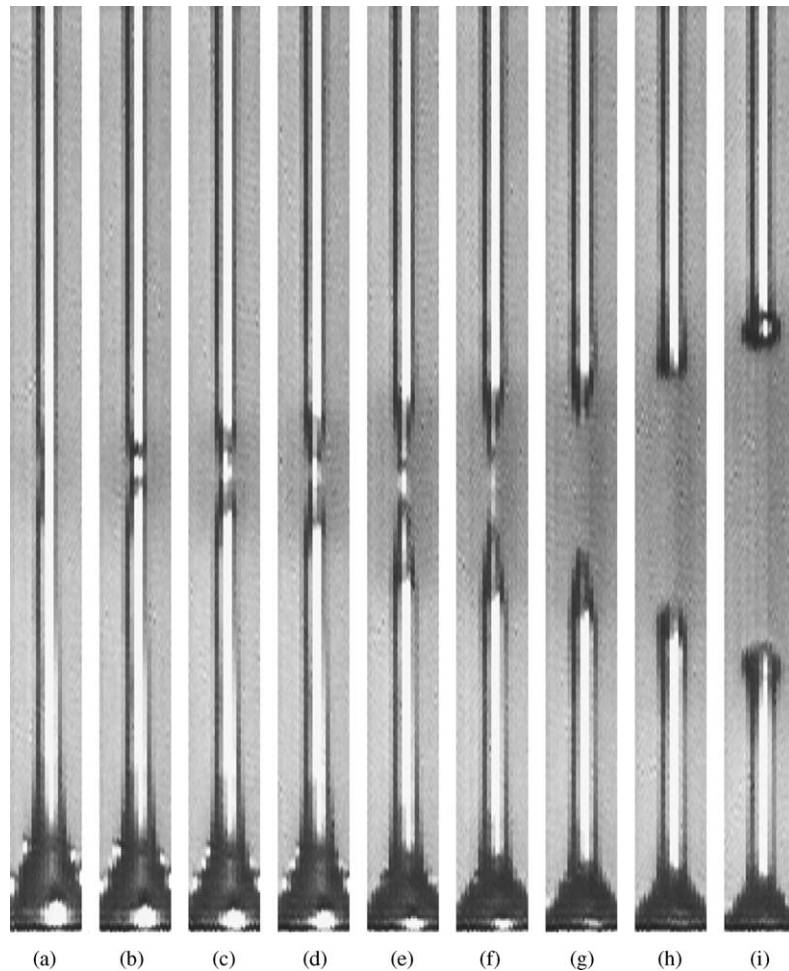


Fig. 4. Close-up of the pinch-off dynamics for 6 mM CTAB/NaSal. The relative times of each image are (a) 0 ms, (b) 5 ms, (c) 8 ms, (d) 10 ms, (e) 16 ms, (f) 18 ms, (g) 20 ms, (h) 22 ms, and (i) 24 ms. The resolution is 0.15 mm per pixel. The size of each image is 0.24 cm  $\times$  3.27 cm.

previously reported in concentrated polymer filaments [39,40] (see also [41]). After pinch-off, the free filament ends retract stably to the drop or orifice, with no satellite drop formation.

A detailed view of the pinching event is shown for a different experiment with the same fluid in Fig. 4. This sequence of images show that the primary filament tapers down to a secondary filament in a localized region; the breakup then occurs along this finer secondary filament, between frames (f) and (g). In the frame before pinch-off, the diameter of the primary and secondary filaments are 0.6 and 0.1 mm and the length of the secondary filament is 2.4 mm. The entire breaking event takes place in about 20 ms, and generally occurs on the order of tens of milliseconds in our experiments. The length of the filament and the location at which it breaks varies from drop to drop, and it is not clear what is the specific cause of the failure in each case. The response of the solution after pinch-off is fluid-like, in that the free ends of the filament form spherical caps (see Fig. 4(i)) and the retraction follows.

It appears from Figs. 3 and 4 that on the macroscopic scale the pinch-off instability does not affect the rest of the filament. This is in contrast to the standard capillary-driven pinch-off of a Newtonian fluid [42] studied theoretically by Rayleigh [43] for jets in air and recently by others for drops in air [20–22]. Note that this is also very different than the instability of liquid-liquid systems, as studied for instance by Tomotika [44] and Meister and Scheele [45]. It has been shown experimentally that the pinch-off of low viscosity Newtonian fluids occurs at the filament's connection to the drop and orifice (termed “end-pinching”) [21]. For higher viscosity fluids, the filament grows longer and perturbations develop along its interface; the filament ultimately breaks somewhere between these perturbations (termed “internal-pinching”). A filament's stability to perturbations determines whether a fluid will end-pinch, producing just one satellite drop, or internally-pinch, producing several satellite drops [22].

While end-pinching is also a localized instability, it is clear from Figs. 3 and 4 that the micellar fluid ruptures along the interior of the filament rather than at the ends. The pinch-off is also very different from internal-pinching since the filament remains cylindrical away from the instability. The rupture of this micellar filament is also different from the standard bead-on-string mode of instability characteristic of some polymer fluids [24,25]. The manner in which the micellar filament breaks generates no satellite drops, which may be an important aspect for use in controlled flow processes.

Although we do not yet understand the mechanism for this localized filament rupture, there are a few studies of simple one-dimensional models for the stretching of a viscoelastic filament that may be related, though the connection to micellar fluids is not clear. In simulations of a simple model using the upper convected Jeffreys equation, Markovich and Renardy [23] found rapid growth in the axial strain at the top of the filament, which they interpret would result in localized pinch-off of the filament. In a different study with a slender body model based on the Maxwell equation, Wang et al. [46] found the onset of a change of type instability which they conjecture should also coincide with a localized filament failure. Furthermore, they found the location of this instability could develop anywhere along the filament and did not necessarily coincide with the filament's thinnest region. While it may be that the pinch-off of a wormlike micellar filament is due to accelerated growth of the axial strain in a localized region, or to a change of type instability, the cause of this instability is still an open question which remains for future investigation.

### 3.2. 80 mM CPCl/60 mM NaSal

The dynamics of the falling drop, pinch-off and filament retraction for the 80 mM CPCl/60 mM NaSal solution are by comparison quite different than the CTAB solution discussed above. Fig. 5 shows initially the filament is smooth and cylindrical until the drop slows down, between frames (b) and (c), and fluid begins to accumulate near the lower end of the filament, as if the filament is slowly draining. Subsequently, the filament is no longer cylindrical and the interface develops a roughened surface that tapers asymmetrically down to a thinner secondary thread approximately 3.5 cm from the orifice. The filament pinches off along this thinner thread between frames (e) and (f). This entire breaking event, from a cylindrical filament to pinch-off, occurs over a longer time interval, on the order of seconds compared to the tens of milliseconds time scale for the lower concentration CTAB solution. Immediately after pinch-off, the solution acts solid-like in the sense that the free ends of the filament curl rather than ball up. These images suggest that sometime during the extensional stretching of the filament a transition to a gel-like phase has occurred. Shear-induced transitions to a gel phase have indeed been seen in wormlike micellar solutions [10].

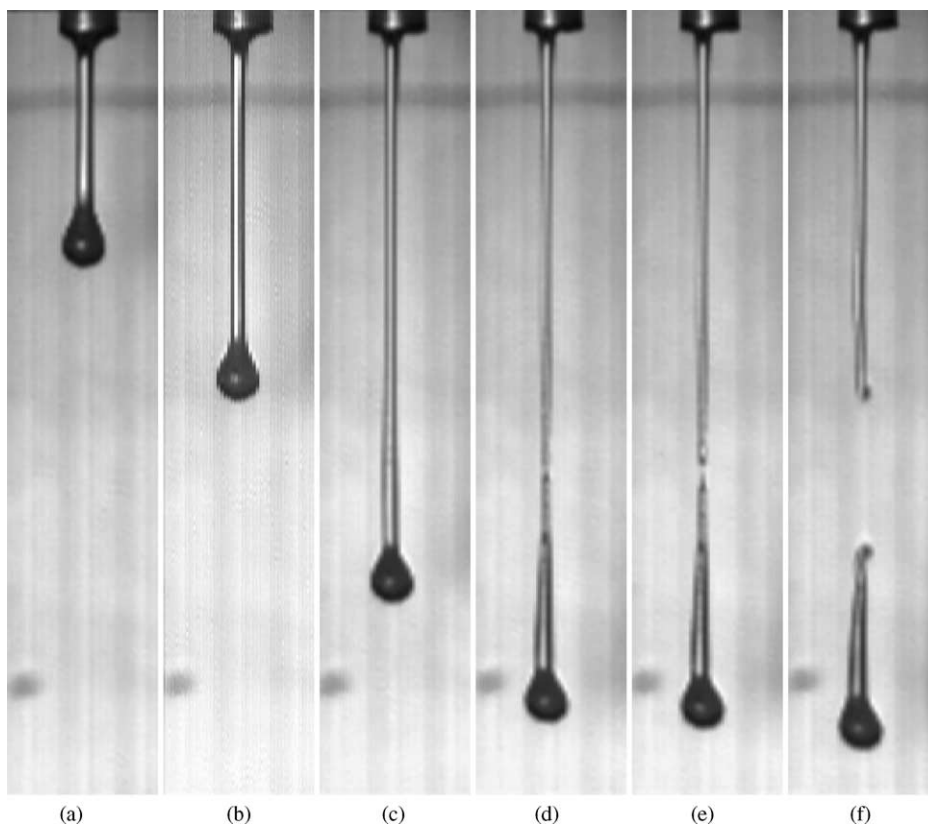


Fig. 5. The pinch-off of a falling drop of an aqueous solution of 80 mM CPCl/60 mM NaSal; the relative times of each image are (a) 0 s, (b) 1.492 s, (c) 4.324 s, (d) 5.500 s, (e) 5.506 s, and (f) 5.520 s. The resolution is 0.26 mm per pixel. The size of each image is 1.7 cm  $\times$  6.3 cm.

Fig. 6 shows that after pinch-off the free filament connected to the orifice snaps back like a rubber band, coiling as it moves towards the orifice, then relaxing downwards to form an eyelet at its free end. The filament continues to oscillate up and down, damping to its final configuration which is approximately 1.4 cm long. The inability of the filament to fully retract back into the orifice precipitates the coiling action, displaying a memory of the stress imposed during its initial extension. Similar solid-like filaments have been seen by McKinley in an extensional rheometry experiment using the associating polymer system HEUR [47].

### 3.3. 100 mM CPCl/60 mM NaSal

The 100 mM CPCl/60 mM NaSal solution, which is the most elastic of the three micellar solutions, develops a surface instability during the stretch of the filament. The initially smooth interface becomes rough as the filament stretches, shown in Fig. 7(a); here, the filament is approximately 0.6 mm wide. As the filament continues to extend, this roughness develops into a distinctly bumpy texture which we refer to as *surface blistering* (Fig. 7(b) and (c)) with the diameter ranging between 0.2 and 0.5 mm in frame

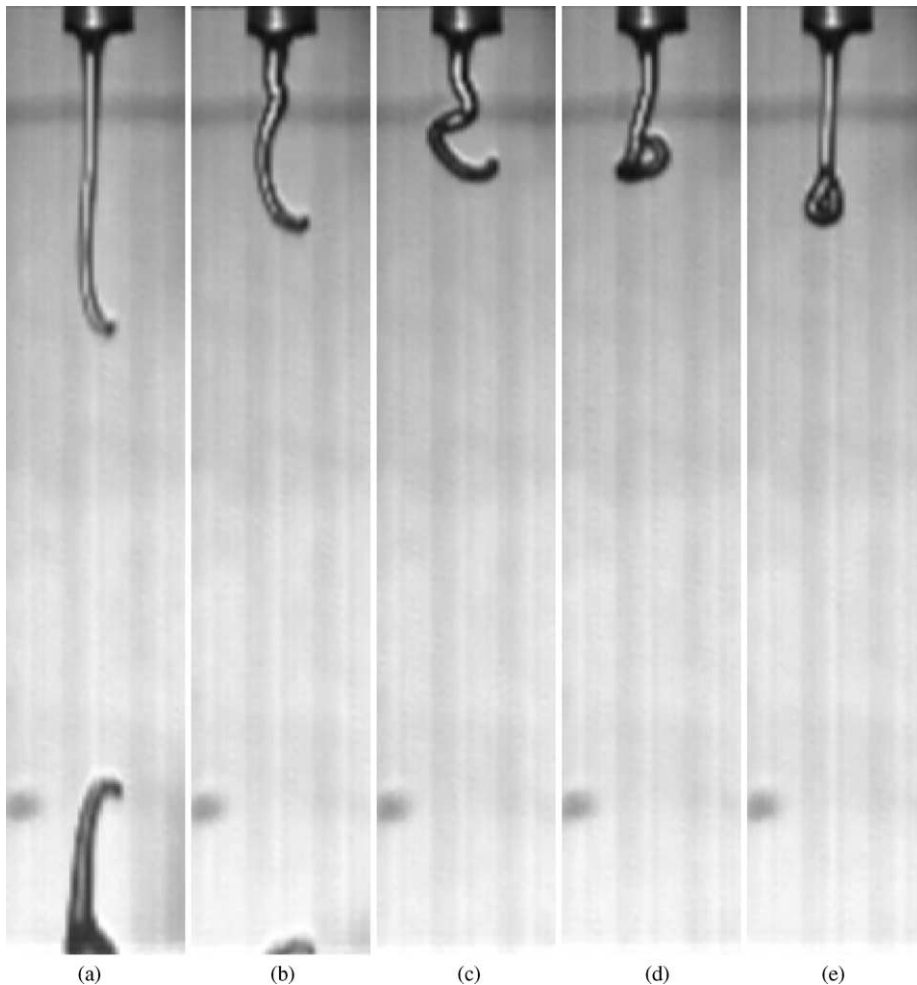


Fig. 6. Dynamics of the broken filament after pinch-off (continuation of Fig. 5 after 20 ms have elapsed), 80 mM CPCl/60 mM NaSal; the relative times of each image are (a) 0 ms, (b) 18 ms, (c) 32 ms, (d) 52 ms, and (e) 218 ms. The resolution is 0.26 mm per pixel. The size of each image is 1.7 cm  $\times$  6.3 cm.

(c). Although we do not yet understand the origin of this blistering, it is reminiscent of two different behaviors that exhibit similar morphologies: (i) the sharkskin instability [48,49] and (ii) a shear-induced sponge-like structure [31]. The sharkskin instability is characterized by a surface roughness, with length scale of about 100  $\mu\text{m}$ , that develops as a molten polymer is extruded from a die. It is commonly believed that wall slip between the polymer and the die is important to the onset of this instability [48,49]. In the second example, wormlike micellar solutions in a shear flow are seen to form patches of new structures, described as “sponge-like bumps” and a “cracked parched-earth texture”. These large structures, which are hundreds of microns in size, are richer in surfactant solution than the background fluid, which leads to the interesting morphology [31]. The length scales of these two instabilities are comparable to the filament diameter in our experiments. This leads us to conjecture that surface blistering may be related to one of them, a subject for further investigation.

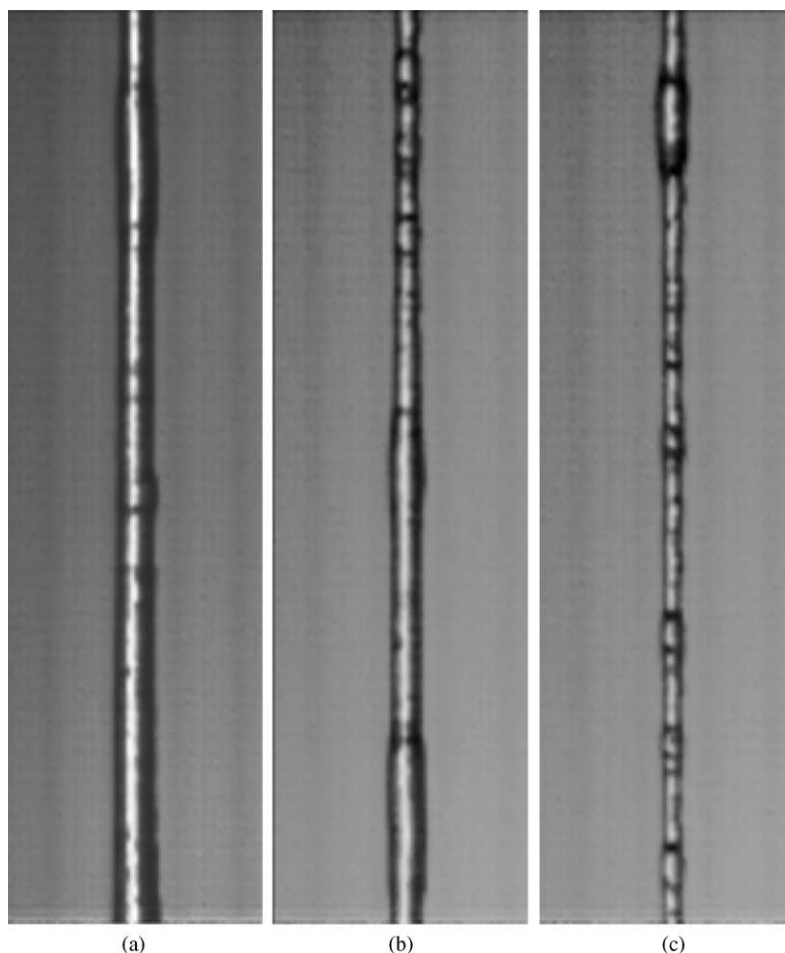


Fig. 7. Detail of texture on the surface of a filament of a falling drop of an aqueous solution of 100 mM CPCI/60 mM NaSal; the relative times of each image are (a) 0 s, (b) 0.85 s, and (c) 1.31 s. The resolution is 0.07 mm per pixel. The size of each image is 0.54 cm  $\times$  1.62 cm.

The breakup of the filament occurs locally as in the filaments of the previous two fluids. Once again, the filament thins to a finer thread along which breakup occurs, as shown in Fig. 8. The response of the free filament after breakup is solid-like; the free ends curl but do not fully retract under the accumulated stress imposed during the extension of the filament. This behavior is very similar to the 80 mM CPCI/60 mM NaSal solution.

#### 4. Drop length dynamics

Another view of the pinch-off process is provided by measuring the changing length of the drop  $L(t)$ , defined as the distance from the orifice to the bottom end of the drop. Fig. 9 compares two fluids: (a)

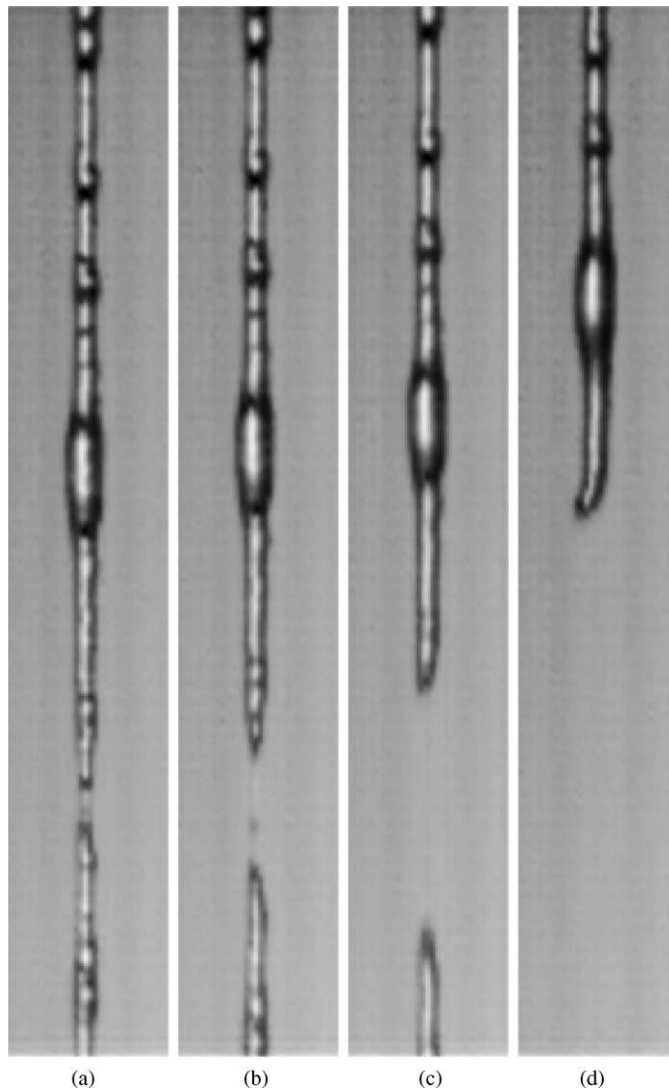


Fig. 8. Close-up of the pinch-off dynamics of 100 mM CPCI/60 mM NaSal solution (continuation of Fig. 7 after 0.2 s have elapsed); the relative times of each image are (a) 0 ms, (b) 2 ms, (c) 3.3 ms, and (d) 7 ms. The resolution is 0.07 mm per pixel. The size of each image is 0.29 cm  $\times$  1.62 cm.

a standard polymer solution, 0.08% xanthan gum/0.39% KCl in 80:20 glycerol/water [50], and (b) the 6 mM CTAB/NaSal solution. Although the rates at which the drops fall are different for these two fluids, their behavior is quite similar. Comparisons of  $L(t)$  to the distance an object free falls with the same initial data (solid line) indicate the filament retards the fall of the drop, an effect which is slightly more pronounced for the micellar solution in this case.

The response of the 6 mM CTAB/NaSal solution after pinch-off is fluid-like, in that the filament fully retracts back into either the drop or the orifice. Measurements of the filament length, for the filament

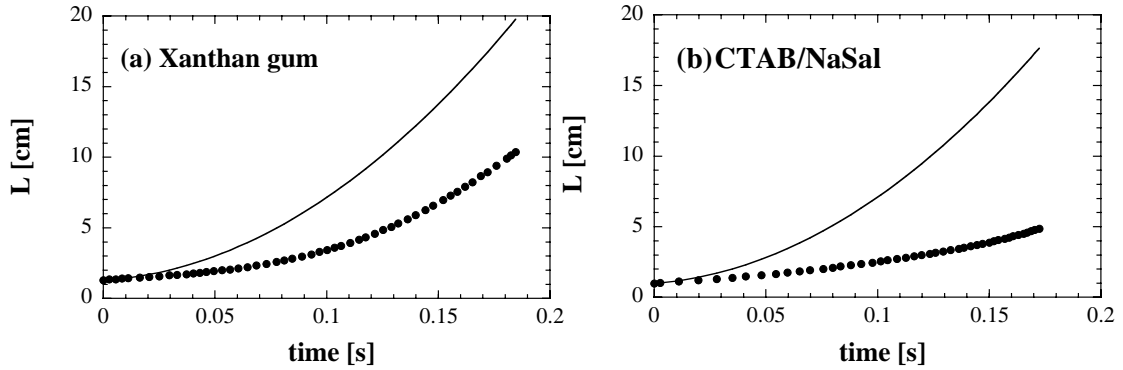


Fig. 9. Drop length vs. time for: (a) 0.08% xanthan gum/0.39% KCl in 80:20 glycerol/water, and (b) 6 mM CTAB/NaSal solution. The data is denoted by circles, and the solid curve represents a drop in free fall with the same initial length and velocity as the data: (a)  $L(0) = 1.3$  cm,  $L'(0) = 17.0$  cm/s; (b)  $L(0) = 1.0$  cm,  $L'(0) = 16.5$  cm/s.

connected to the orifice, are provided in Fig. 10 corresponding to the experiment in Fig. 3 (after frame (d)). This stable retraction process is also commonly observed for elastic polymer solutions [40,50].

Measurements of the drop length for the 80 mM CPCl/60 mM NaSal solution are shown in Fig. 11 for four experiments which represent the range of behavior we observed. In all of the experiments the drop initially stretches at a nearly constant velocity, varying between 0.15 and 0.78 cm/s. After this initial stage, the dynamics vary among the following three scenarios. In the first case (Fig. 11(a)), the drop suddenly accelerates as the perturbation appears; breakup of the filament results. In the second case (Fig. 11(b) and (c)), which occurs most often, the drops briefly slowed down before acceleration occurred. Finally, in the third case (Fig. 11(d)), which is the most intriguing, the drop actually stopped momentarily before acceleration and breakup. We refer to this as *stall*. Note that the drop is held stationary for one full second, this is remarkably long compared to the milliseconds-long time scale for pinch-off. Based on the data in Fig. 11, we calculate the Hencky strain

$$\epsilon = \int_0^t \dot{\epsilon}(\tau) d\tau$$

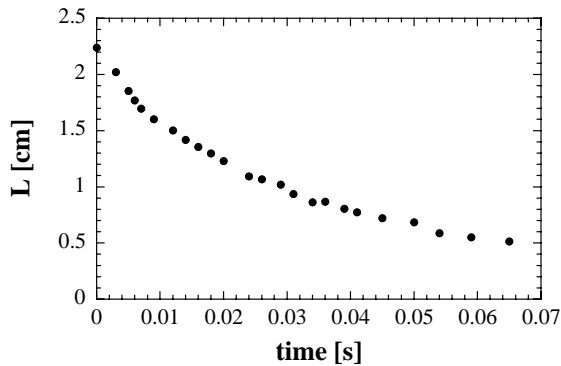


Fig. 10. Length vs. time of the retracting free filament, measured from the orifice to the filament tip, for the 6 mM CTAB/NaSal solution. Data corresponds to the experiment in Fig. 3 after frame (d).

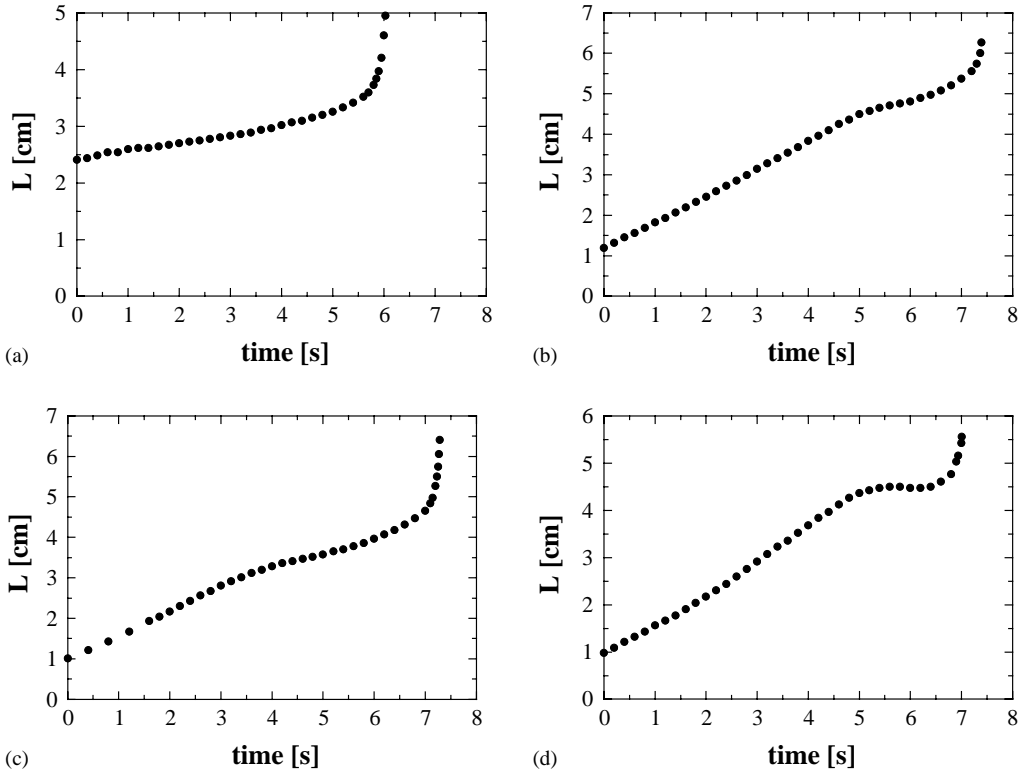


Fig. 11. Length vs. time for solution of 80 mM CPCI/60 mM NaSal in four different cases. The data in (d) corresponds to the drop shown in Fig. 5. The stretch rate and Hencky strain during the period of linear growth (see text): (a)  $\dot{\epsilon} = 0.05 \text{ s}^{-1}$ ,  $\epsilon = 1.12$ ; (b)  $\dot{\epsilon} = 0.15 \text{ s}^{-1}$ ,  $\epsilon = 1.50$ ; (c)  $\dot{\epsilon} = 0.19 \text{ s}^{-1}$ ,  $\epsilon = 1.15$ ; and (d)  $\dot{\epsilon} = 0.16 \text{ s}^{-1}$ ,  $\epsilon = 1.47$ .

over the period of linear growth of  $L(t)$  and the stretch rate

$$\dot{\epsilon}(t) = \frac{1}{L} \frac{dL}{dt}$$

at the end of the period of linear growth; these values are shown in the figure caption. We do not see a simple correlation between either the stretch rate or strain and the type of dynamics leading to pinch-off, which would differentiate between Fig. 11(a)—no slow down before pinch-off, Fig. 11(b) and (c)—slow down before pinch-off, and Fig. 11(d)—complete stall before pinch-off. We note however that comparing values of the strain is somewhat arbitrary since the experiments were not synchronized to the same initial length at  $t = 0$ . In all of the experiments we conducted, the stretch rate over the whole linear period ranged between  $0.05$  and  $0.21 \text{ s}^{-1}$  and the calculated strain ranged between  $0.92$  and  $1.63$ .

Our focus in the remainder of this paper will be on the phenomena of stall. We conjecture that it is the accumulated elastic stress in the filament that is responsible for this stall. In Section 5, we investigate a model that qualitatively supports this idea.

## 5. Discussion and modeling

The images of the onset and growth of the filament perturbations which lead to drop pinch-off in these micellar fluids suggest that a localized mechanism is responsible for the breaking. This behavior may be related to the change of type instability in a stretching filament as seen by Wang et al. in their simulations of a one-dimensional Maxwell model [46], or by the unbounded growth of the axial strain observed by Markovich and Renardy [23] in their one-dimensional Jeffreys model, though the specific connection to wormlike micellar fluids is unclear. In addition, at higher surfactant concentrations the filament itself appears to undergo various changes such as gelling and surface blistering. A full understanding of these different effects may require knowledge of the specific rheological properties of wormlike micellar solutions, and though there are some successful constitutive models for these fluids in simple flows (see, e.g. [2,16]), they are not appropriate to the transient extensional flows considered here. We leave the theoretical treatment of these instabilities to future work, and focus instead on another surprising observation, the stall of the falling drop.

The arrested fall of a micellar drop which we observed in the CPC1 solution, shown in Fig. 11(d), is remarkably long lived. We know of only one other observation of stalling drops, made by Jones et al. with the Boger fluid M1 [51]; their data show a stall for about 0.02 s. These measurements were qualitatively reproduced in a simple model for the drop length by Keiller [1], using a form of the Oldroyd-B constitutive equation. Here, we generalize Keiller's model by using the FENE-CR constitutive equation, and make a detailed study of the stall phenomenon in terms of the forces which slow down the drop, and the dependence of this process on the parameters. We first derive this model based on several simplifying assumptions, then briefly discuss some of these assumptions in terms of what is known about wormlike micellar fluids, before presenting the results.

### 5.1. A simplified model

To begin, we approximate the fluid filament as a cylinder of radius  $h(t)$  surrounded by a passive ambient atmosphere, with a sphere of mass  $M$  attached at the lower filament boundary  $z = L(t)$ ;  $z$  is referenced from the top of the filament, see Fig. 12. Note that for convenience we are redefining the drop length, differently from what was used in the experiments. In the model, the drop/filament length is measured from the orifice to the end of the filament, thus the two definitions differ by the diameter of the drop. Since the drop diameter is nearly constant in the experiments while  $L(t)$  is measured, the two definitions differ only by a constant. The filament is assumed to be in a purely extensional flow, which for an incompressible fluid is described by  $\mathbf{u} = (-\dot{\epsilon}r/2, 0, \dot{\epsilon}z)$ , where  $\dot{\epsilon}$  is the stretch rate. The kinematic boundary condition at the filament end ( $z = L$ ) is

$$\dot{\epsilon}L = \frac{dL}{dt}. \quad (2)$$

Since the filament is fixed at  $z = 0$  where the axial velocity is zero, and no fluid can flow out at  $z = L$  due to the kinematic condition, the volume of the filament  $V_0$  must be constant. This allows the filament radius to be expressed in terms of its length by  $h(t) = \sqrt{V_0/\pi L(t)}$ . The kinematic boundary condition also ensures that the mass of the sphere  $M$  is constant.

The forces acting on the filament at  $z = L$  are the gravitational force due to the sphere, a surface tension force resulting from the connection of the sphere to the filament, and a force due to axial stresses in the

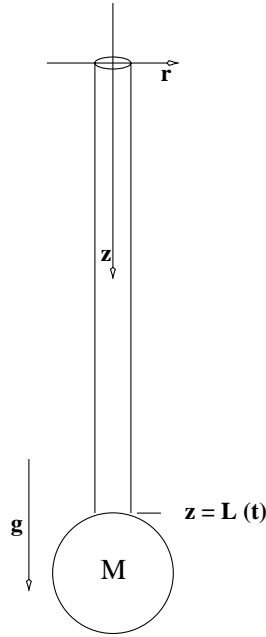


Fig. 12. Schematic of a cylindrical filament connected to a spherical drop of constant mass.

filament; the weight of the filament is neglected. Thus, the force balance at  $z = L$  is

$$M \frac{d^2 L}{dt^2} = Mg - 2\pi h \gamma - F_f, \quad (3)$$

with the force due to the filament stress described by  $F_f = (\sigma_{zz} - p)\pi h^2$ , where  $\gamma$  is the constant surface tension (discussed below),  $\sigma_{zz}$  is the axial extra stress component and  $p$  is the pressure. We determine the pressure using the normal stress condition at the filament interface,  $\hat{n} \cdot \mathbf{T} \cdot \hat{n} = -\gamma\kappa$ , where  $\hat{n}$  is the normal vector to the surface,  $\mathbf{T}$  is the total stress tensor and  $\kappa = 1/h(t)$  is the curvature of the filament. Because an extensional flow has no shear, the normal stress condition reduces to  $p = \sigma_{rr} + \gamma/h(t)$ , where  $\sigma_{rr}$  is the radial extra stress component. Substituting this pressure into the force equation yields

$$F_f = \left( \sigma_{zz} - \sigma_{rr} - \frac{\gamma}{h} \right) \pi h^2. \quad (4)$$

We write the extra stress in terms of the FENE-CR constitutive equation [26], which is a simplified version of the FENE dumbbell model [52]. This constitutive model contains stress contributions from the Newtonian solvent (viscous term) and the polymer (elastic term)

$$\sigma = 2\eta \mathbf{D} + f(R)GA, \quad (5)$$

where  $\eta$  is the dynamic shear viscosity,  $\mathbf{D} = (\nabla \mathbf{u} + \nabla \mathbf{u}^T)/2$  is the symmetric part of the velocity gradient tensor,  $G$  is the elastic modulus,  $\mathbf{A}$  is an elastic strain tensor representing the ensemble average of the dyadic product  $\mathbf{R}\mathbf{R}$  of the dumbbell end-to-end vector  $\mathbf{R}$  [26], and  $f(R)$  is the non-dimensional spring

force law

$$f(R) = \frac{1}{1 - R^2/b} \quad \text{where } R^2 \equiv \text{tr}(\mathbf{A}). \quad (6)$$

The parameter  $b$  is the square of the ratio of the length of the fully extended dumbbell (or molecule) to its equilibrium length [26]. The strain tensor  $\mathbf{A}$  satisfies

$$\frac{D\mathbf{A}}{Dt} = \mathbf{A} \cdot \nabla \mathbf{u} + \nabla \mathbf{u}^T \cdot \mathbf{A} - \frac{f(R)}{\lambda} (\mathbf{A} - \mathbf{I}), \quad (7)$$

where  $\lambda$  is the relaxation time and  $\mathbf{I}$  is the identity tensor. As  $b \rightarrow \infty$ , the spring force  $f(R) \rightarrow 1$ ; in this limit, the FENE-CR model (5)–(7) reduces to a form of the Oldroyd-B equation. In strong extensional flows, the Oldroyd-B equation can numerically develop infinite stresses resulting from the infinitely extensible dumbbells. The nonlinear spring force in the FENE-CR model corrects this by giving a finite limit to the dumbbell extension, and thus to the extensional stress of the fluid [53].

Using Eqs. (5) and (6) for a purely extensional, axisymmetric flow we have

$$\sigma_{zz} - \sigma_{rr} = 3\eta\dot{\epsilon} + \frac{G(a_{zz} - a_{rr})}{1 - (a_{zz} + 2a_{rr})/b}, \quad (8)$$

where the axial and radial deformations follow

$$\frac{da_{zz}}{dt} = 2\dot{\epsilon}a_{zz} - \frac{a_{zz} - 1}{\lambda[1 - (a_{zz} + 2a_{rr})/b]}, \quad (9)$$

$$\frac{da_{rr}}{dt} = -\dot{\epsilon}a_{rr} - \frac{a_{rr} - 1}{\lambda[1 - (a_{zz} + 2a_{rr})/b]}, \quad (10)$$

where we assume the strain tensor is spatially independent. Using (4) and (8) in the force balance (3) results in

$$M \frac{d^2L}{dt^2} = Mg - \gamma\pi h - \left( 3\eta\dot{\epsilon} + \frac{G(a_{zz} - a_{rr})}{1 - (a_{zz} + 2a_{rr})/b} \right) \pi h^2, \quad (11)$$

which can be expressed in terms of  $L$  using the definition of  $h(t)$  and the kinematic condition for  $\dot{\epsilon}$  as

$$M \frac{d^2L}{dt^2} = Mg - \gamma\sqrt{\frac{V_0\pi}{L}} - \frac{3\eta V_0}{L^2} \frac{dL}{dt} - \frac{V_0 G}{L} \left( \frac{a_{zz} - a_{rr}}{1 - (a_{zz} + 2a_{rr})/b} \right). \quad (12)$$

Similarly, (9) and (10) can be written as

$$\frac{da_{zz}}{dt} = \frac{2}{L} \frac{dL}{dt} a_{zz} - \frac{a_{zz} - 1}{\lambda[1 - (a_{zz} + 2a_{rr})/b]}, \quad (13)$$

$$\frac{da_{rr}}{dt} = -\frac{1}{L} \frac{dL}{dt} a_{rr} - \frac{a_{rr} - 1}{\lambda[1 - (a_{zz} + 2a_{rr})/b]}. \quad (14)$$

## 5.2. Connecting the model to wormlike micellar fluids

Eqs. (12)–(14) form a coupled system of ODEs that define a simplified model for the extensional flow of a filament connected to a falling drop. We numerically solve these equations and discuss the parameters

for which a stall is observed. For initial conditions we follow [1], with  $L(0) = 0.1$  cm,  $L'(0) = 0$ ,  $V_0 = 0.0126$  cm<sup>3</sup> and  $a_{zz}(0) = a_{rr}(0) = 1$ . The density of our wormlike micellar fluids is typically  $\rho = 1.0$  g/cm<sup>3</sup> [13]. The observation of stall which originally motivated this model was made in the 80 mM CPCI/60 mM NaSal solution, for which we have measured a relaxation time of 1.7 s, a zero shear viscosity of 430 P, and an elastic modulus of 220 dyn/cm<sup>2</sup>; these values are intermediate between the other two fluids we have studied. However, for comparison purposes we will use the same parameter values as Keiller ( $\lambda = 0.3$  s,  $\eta = 16.7$  P and  $G = 35$  dyn/cm<sup>2</sup> [1]), which are not far from the fluids studied here.

In deriving our simplified model (12)–(14), we have assumed that the surface tension  $\gamma$  is constant. However, it would not be at all surprising if there were dynamic surface tension effects, as the viscoelastic fluid is comprised of surfactant aggregations. While such effects are probably present at some level in all of the phenomena we have observed, it is less likely that they play an essential role in the stall of falling drops; such dynamic effects may however be important to the surface blistering (Figs. 7 and 8). We have made the simplifying assumption that  $\gamma$  is constant, using the value  $\gamma = 36$  dyn/cm reproducibly measured for 11 mM CTAB/NaSal in air [13]. Our model allows for the inclusion of dynamic surface tension effects, which would in principle couple another ordinary differential equation to (12).

Estimating the FENE-CR parameter  $b$  for a wormlike micellar fluid is difficult since the lengths of the micelles are continuously changing. In the kinetic theory of polymers  $b \sim 3N$  where  $N$  is the number of Kuhn steps along the molecule [52]. An estimate for  $b$  can be made by approximating  $N$  as the ratio of the micelle's characteristic length in a quiescent state ( $\sim 1$   $\mu$ m) [31] to its persistence length ( $\sim 10$  nm) [28], which gives  $N \sim 100$  ( $b \sim 300$ ). As we will see later, this is close to the lower limit of the stall phenomenon in our model; in order to separate the FENE effects from the other factors in our model, we somewhat arbitrarily set  $b = 10,000$  for most of our numerical simulations.

### 5.3. Results

We find in numerical simulations of (12)–(14) that for small values of the mass  $M$  the forces that oppose gravity significantly inhibit the fall of the drop, whereas for large values of  $M$  the drop is almost in free fall. Furthermore, there exists a range of mass,  $0.063$  g  $\leq M \leq 0.160$  g, for which the filament stalls, an example of which is shown in Fig. 13 with  $M = 0.11$  g. We define stall to occur when  $L'(t) = 0$ .

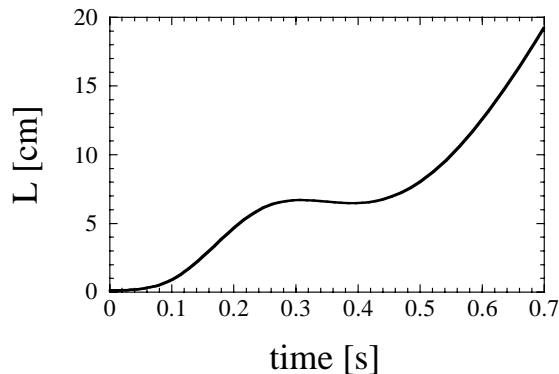


Fig. 13. Filament length vs. time for  $M = 0.11$  g using Eqs. (12)–(14) with  $b = 10,000$ ,  $\eta = 16.7$  P and  $G = 35$  dyn/cm<sup>2</sup>.

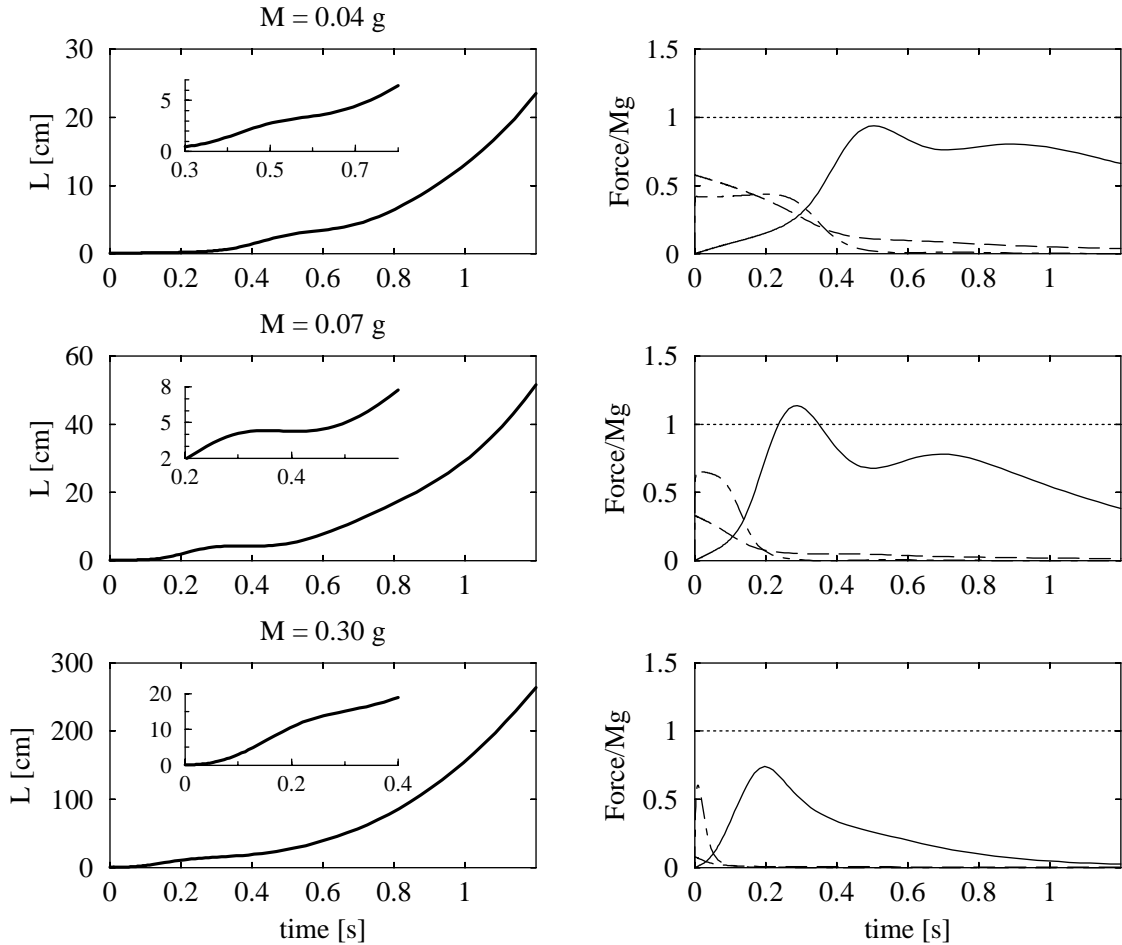


Fig. 14. Filament length vs. time and the corresponding normalized force budgets for  $M = 0.04, 0.07$  and  $0.30$  g using Eqs. (12)–(14) with  $b = 10,000$ ,  $\eta = 16.7$  P and  $G = 35$  dyn/cm<sup>2</sup>. Insets show close-up of length vs. time. In the budgets: gravitational force (dotted), surface tension force (dashed), viscous force (dot-dashed) and elastic force (solid).

In the simulations, the range of mass for stall is not sensitive to the initial velocity. Using the maximum initial velocity measured in the experiments with the 80 mM CPCI/60 mM NaSal solution (0.78 cm/s) as  $L'(0)$ , we find the range of mass for stall is still the same. The length of the filament varies only slightly with the initial velocity:  $L(0.7) = 20.48$  cm when we let  $L'(0) = 0.78$  cm/s in the numerical simulation, which is 0.7% larger than  $L(0.7)$  with zero initial velocity shown in Fig. 13. All simulations are therefore performed with  $L'(0) = 0$ .

Fig. 14 shows the filament length and the corresponding force budgets for  $M = 0.04, 0.07$  and  $0.30$  g to illustrate the relative importance of each term in the force balance and their dependence on the mass of the drop. The force budgets show the magnitude of each term in (12) normalized by the weight of the drop. For relatively small mass,  $M = 0.04$  g, the filament initially stretches slowly as the surface tension and viscous forces oppose the fall of the drop. After a transient period these terms decay and

the elastic force increases to a value just below the gravitational force. This growth in the elastic force decreases the filament velocity at  $t \approx 0.43$  s, but does not cause a complete stall. At an intermediate value,  $M = 0.07$  g, the viscous and surface tension forces decay more rapidly and have a negligible effect on the initial stretch of the filament. Meanwhile, the growth rate and maximum of the elastic force are significantly larger, which is enough to stall the drop for approximately 0.06 s. This effect is short-lived as the elastic force decays and the velocity of the filament increases. For a larger mass,  $M = 0.30$  g, the viscous and surface tension forces are negligible and the elastic force grows to a maximum over a brief time interval. The magnitude of the elastic force is significantly less than the gravitational force, thus during this time period the elastic force resists the stretching of the filament, although not enough to stall the drop. In summary, Fig. 14 shows that stall occurs when the elastic force balances the weight of the drop.

In an analysis of a similar filament model using the Oldroyd-B constitutive equation ( $b \rightarrow \infty$ ), Keiller identifies the initial growth of the filament as viscous dominated [1]. He also estimates that if the Deborah number, which is the ratio of the relaxation time to a characteristic flow time, begins and remains sufficiently large, then the elastic force grows comparable to the weight of the drop. Comparing various defined stretch parameters, Keiller provides criteria as to whether the transition from the viscous to elastic dominated phases will be smooth, causing no stall, or more abrupt, resulting in a slow down or even bouncing of the drop; this elastic phase continues until  $L'' \approx g$ .

Here, we have observed stall in a model using the FENE-CR equation. This is a common constitutive model used for dilute polymer solutions, yet stall in a falling drop has not been widely reported in physical systems. We are aware of two fluids for which drops stall: the M1 fluid [51] and the 80 mM CPCl/60 mM NaSal solution reported here. Some examples of fluids that do not stall are the xanthan gum [50] and 6 mM CTAB/NaSal solutions reported herein (Fig. 9) and the solution FM9 in kerosene [40]. One may wonder why some solutions stall while others do not. We investigate this phenomena by examining the parameter dependence of the FENE-CR model, and find qualitative evidence that the occurrence of stall is determined by the fluid viscosity, elasticity and relaxation time. We show this by identifying the regions of parameter space in which stall is observed.

To generalize the interplay between the viscous, elastic and relaxational effects on the dynamics of stall, we non-dimensionalize our model (12)–(14). Using the length and time scales,  $L_0$  and  $\sqrt{L_0/g}$  (where  $L_0 = L(0)$ ), to define the dimensionless quantities

$$\hat{L} = \frac{L}{L_0} \quad \text{and} \quad \hat{t} = \frac{t}{\sqrt{L_0/g}},$$

results in the non-dimensional form of (12):

$$\frac{d^2 \hat{L}}{d\hat{t}^2} = 1 - \frac{1}{Bo} \sqrt{\frac{1}{\hat{L}}} - \frac{1}{Re} \frac{1}{\hat{L}^2} \frac{d\hat{L}}{d\hat{t}} - \frac{1}{\Omega} \frac{1}{\hat{L}} \left( \frac{a_{zz} - a_{rr}}{1 - (a_{zz} + 2a_{rr})/b} \right), \quad (15)$$

where the dimensionless groups are the Bond number,

$$Bo = \frac{Mg}{\gamma} \sqrt{\frac{L_0}{V_0\pi}},$$

which measures the importance of gravitational to surface tension forces; an effective Reynolds number,

$$Re = \frac{MU_0L_0}{3\eta V_0},$$

(where  $U_0 = \sqrt{gL_0}$ ), which measures the importance of inertial to viscous forces; and an elastic Bond number,

$$\Omega = \frac{MgL_0}{GV_0},$$

which measures the importance of gravitational to elastic forces. The non-dimensional form of (13) and (14) are given by

$$\frac{da_{zz}}{d\hat{t}} = \frac{2}{\hat{L}} \frac{d\hat{L}}{d\hat{t}} a_{zz} - \frac{1}{De} \left( \frac{a_{zz} - 1}{1 - (a_{zz} + 2a_{rr})/b} \right), \quad (16)$$

$$\frac{da_{rr}}{d\hat{t}} = -\frac{1}{\hat{L}} \frac{d\hat{L}}{d\hat{t}} a_{rr} - \frac{1}{De} \left( \frac{a_{rr} - 1}{1 - (a_{zz} + 2a_{rr})/b} \right), \quad (17)$$

where

$$De = \lambda \sqrt{\frac{g}{L_0}},$$

denotes the Deborah number, which compares the relaxation time of the fluid to a characteristic flow time. For our chosen parameters,  $De = 30$ ; this Deborah number is artificially large due to the choice of time scale. We solve the coupled system of non-dimensional Eqs. (15)–(17) numerically and examine the dependence of stall on the Reynolds number, the Deborah number and the parameter  $b$ , each as a function of the elastic Bond number. All simulations were run for  $\hat{t} = [0, 120]$ .

Fig. 15(a) shows the parameter region of stall as a function of  $Re$  and  $\Omega$  with  $Bo = 3.5$ ,  $De = 30$ , and  $b = 10,000$ . There are three distinct regions represented in this graph: no stall, stall and multi-stall. The stall region represents values of  $Re$  and  $\Omega$  for which the drop stopped once in its downward descent. The multi-stall region represents values of  $Re$  and  $\Omega$  for which the drop stopped more than once in its

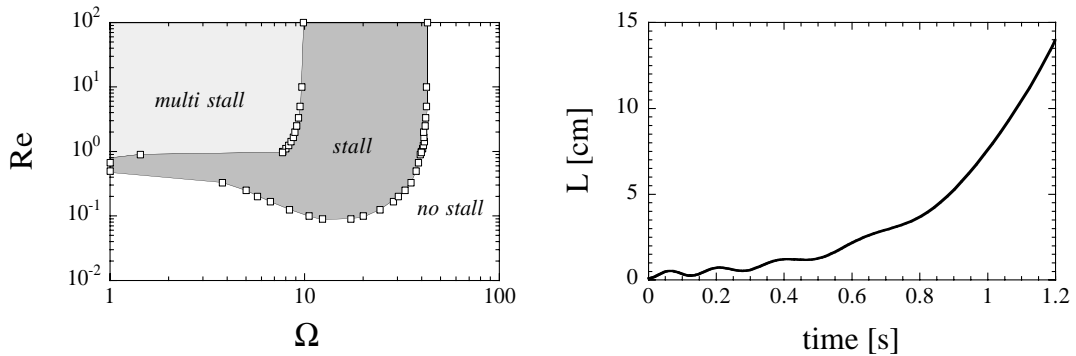


Fig. 15. Drop stall with  $Bo = 3.5$ ,  $De = 30$ , and  $b = 10,000$ : (a) region of stall (shaded area) as a function of  $Re$  and  $\Omega$  calculated using Eqs. (15)–(17); (b) drop length (cm) as a function of time (s) showing multiple stall for  $Re = 5$  and  $\Omega = 3.4$ .

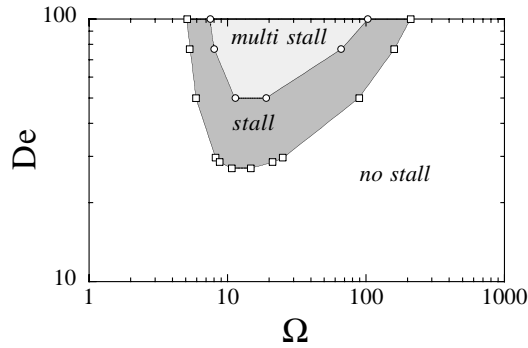


Fig. 16. Region of stall (shaded area) as a function of  $De$  and  $\Omega$  calculated using Eqs. (15)–(17) with  $Bo = 3.5$ ,  $Re = 0.13$ , and  $b = 10,000$ .

downward descent, an example of this behavior is shown in Fig. 15(b) for  $Re = 5$  and  $\Omega = 3.4$ . Notice in Fig. 15(a) that below a critical Reynolds number ( $Re < 0.09$ ) stall does not occur at all. In such a viscous dominated regime, the flow is slow, and as a result the build up and subsequent decay of the elastic stress occurs on a slow time scale. For  $Re \geq 0.09$ , the range of  $\Omega$  for which stall occurs increases with increasing  $Re$ . For sufficiently large  $\Omega$  ( $\Omega \geq 43$ ), in which the gravitational force dominates over the elastic force, stall cannot occur. For lower values of  $\Omega$ , the drop can stall one or more times with the region of multi-stall corresponding to high  $Re$  and low  $\Omega$ . In this case, inertial effects dominate over viscous effects, and elastic effects dominate over gravitational effects. These results indicate that fluids with relatively low viscosity and high elasticity can stall. The phenomena of multiple stalls (elastic oscillations) in falling drops has also been observed by Wang et al. in their simulations of the filament dynamics for a one-dimensional Maxwell model [46], but in the context of filament contraction rather than stretching.

Fig. 16 shows the parameter region of stall as a function of  $De$  and  $\Omega$  with  $Bo = 3.5$ ,  $Re = 0.13$ , and  $b = 10,000$ . The dependence of the model on the relaxation time produces an unbounded region for which the drop stalls. This region is bounded below by a minimum value of the Deborah number ( $De \approx 27.0$ ). Above this critical value, the range of  $\Omega$  for which a stall occurs increases with increasing Deborah number. Notice that drops with sufficiently small or large  $\Omega$  do not stall. In this case, the gravitational force is either too small to build up the elastic stress in the filament, or too large relative to the elastic force. For larger Deborah number ( $De \geq 50$ ) the drop can stall multiple times. Thus, the model predicts that stall occurs in the region of large Deborah number with the gravitational force approximately one to two orders larger than the elastic force.

To interpret the dependence of stall on  $\Omega$ , we compare our fluid drop and filament to a simple undamped mass–spring system. The natural frequency of such a system is  $\omega_{\text{spring}} \sim \sqrt{k/M}$ , where  $k$  is the spring constant and  $M$  is the mass. In a similar manner, we can estimate the natural frequency of a cylindrical elastic spring (i.e. the filament), with initial length  $L_0$  and radius  $h_0$ , by making an order of magnitude estimate for the spring constant as proportional to  $G\pi h_0^2/L_0$ , where  $G$  is the elastic modulus of the filament; from this we have

$$\omega_{\text{spring}} \sim \sqrt{\frac{Gh_0^2/L_0}{M}}.$$

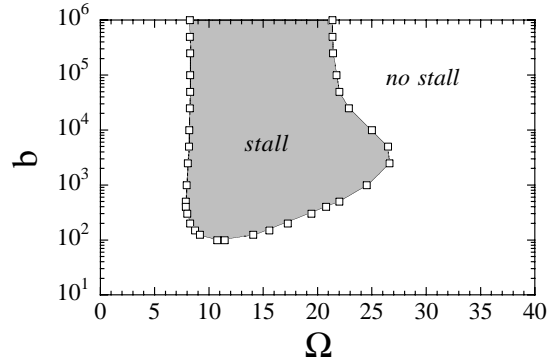


Fig. 17. Region of stall (shaded area) as a function of  $b$  and  $\Omega$  calculated using Eqs. (15)–(17) with  $Bo = 3.5$ ,  $Re = 0.13$ , and  $De = 30$ .

Note that this estimate ignores the dynamical stresses in the filament. We define another frequency using the free fall time,  $\omega_{\text{gravity}} = \sqrt{g/L_0}$ . We expect a resonance to occur in this system when  $\omega_{\text{gravity}} \sim \omega_{\text{spring}}$ . Since

$$\left(\frac{\omega_{\text{gravity}}}{\omega_{\text{spring}}}\right)^2 \sim \frac{MgL_0}{GV_0} = \Omega,$$

the stall of a lengthening elastic filament can by analogy be compared to the parametric resonance in the mass–spring system. The shift in the range of stall for  $\Omega$  from  $O(1)$  to approximately  $O(10)$  (see Fig. 16) may be due to the damping effects (viscosity) included in our model. The multi-stall region may then correspond to higher modes of resonance between the elastic force and the weight of the drop.

Finally, although the parameter  $b$  in (15)–(17) is not really an appropriate quantity for a wormlike micellar fluid, we use it to investigate the effect of finite molecular extensibility on drop stall. Since  $b \sim \text{M.W.}$  [52], it follows that  $b \rightarrow \infty$  would correspond to molecules of infinite length. We vary  $b$  in our model to explore two effects: the possibility of stall in a polymer filament described accurately by the FENE-CR equation, and the elimination of stall due to the limitation on extensional stress imposed by a finite  $b$  value. Fig. 17 shows the parameter region of stall in our model as a function of  $b$  and  $\Omega$  with  $Bo = 3.5$ ,  $Re = 0.13$ , and  $De = 30$ . For large values of  $b$  ( $\geq 250,000$ ), the range of  $\Omega$  for which the filament stalls is uniform,  $8.2 \leq \Omega \leq 21.4$ , thus we interpret  $b \approx 250,000$  as the transition value to finite extensional effects in our model. As the value of  $b$  is decreased below this critical value, the range of  $\Omega$  for stall increases, and is maximal for  $2500 \leq b \leq 5000$ . The region then decreases so that no stall occurs for  $b < 100$ , for any  $\Omega$ . This indicates that a sufficient extensibility (large enough  $b$ ) is required for stall in our model, which would correspond to a lower limit on the molecular weight for a FENE-CR polymer to exhibit stall. Note that, insofar as the assumption of finite extensibility is appropriate for a wormlike micellar fluid, the estimated value  $b \sim 300$  does fall within the observed stall range of our model.

## 6. Conclusions

We have presented several new experimental observations of drops falling through air using aqueous solutions of two standard wormlike micellar solutions, CTAB/NaSal and CPCI/NaSal. We find the instability

that leads to the pinch-off of these wormlike micellar drops is due to a localized phenomenon that is very different from the more common Rayleigh-type (Newtonian fluids) or bead-on-string type (polymer solutions) instabilities. In addition, the manner in which these micellar fluids breaks produces no satellite drops.

The elastic effects of these solutions become more pronounced at higher surfactant concentrations. Experimentally we have observed that: the falling drop can slow down or even stall, the free filament ends recoil after pinch-off with an incomplete retraction, and surface blistering develops along the filament surface. These observations are evidence that the fluid may undergo a transition to a gel-like phase during the filament's downward extension, analogous to the shear-induced transition reported elsewhere [10].

We find the occurrence of stall during the fall of a viscoelastic drop can be understood qualitatively by a simple model based on the FENE-CR constitutive equation. Simulations of the model indicate that stall occurs in the range of low solvent viscosity, high elasticity, and high molecular weight. This is consistent with the properties of wormlike micellar fluids. Qualitatively, the stall of a falling drop can be explained by a resonance condition, that is the time scales of the elasticity and gravity are comparable.

## Acknowledgements

We would like to thank G. McKinley, N.Z. Handzy, and T. Podgorski for enlightening discussions, and A. Bernoff, J.-F. Berret, G. Forest, D.M. Henderson, and M.J. Shelley for helpful comments. AB acknowledges the support of the A.P. Sloan Foundation and National Science Foundation (CAREER Award DMR-0094167). LBS acknowledges the support of the National Science Foundation (VIGRE grant DMS-9983320, and partial support from DMS-0074049) while at Duke University.

## References

- [1] R.A. Keiller, Extending filaments of an Oldroyd fluid, *J. Non-Newtonian Fluid Mech.* 42 (1992) 37–48.
- [2] R.G. Larson, *The Structure and Rheology of Complex Fluids*, Oxford University Press, Oxford, 1999.
- [3] A.S. Wunneburger, A. Colin, J. Leng, A. Arneodo, D. Roux, Oscillating viscosity in a lyotropic lamellar phase under shear flow, *Phys. Rev. Lett.* 86 (2001) 1374–1377.
- [4] D. Bonn, J. Meunier, O. Greffier, A. Al-Kahwaji, H. Kellay, Bistability in non-Newtonian flow: rheology of lyotropic liquid crystals, *Phys. Rev. E* 58 (1998) 2115–2118.
- [5] E. Lemaire, P. Levitz, G. Daccord, H. Van Damme, From viscous fingering to viscoelastic fracturing in colloidal fluids, *Phys. Rev. Lett.* 67 (1991) 2009–2012.
- [6] H. Zhao, J.V. Maher, Associating-polymer effects in a Hele–Shaw experiment, *Phys. Rev. E* 47 (1993) 4278–4283.
- [7] J. Ignés-Mullol, H. Zhao, J.V. Maher, Velocity fluctuations of fracture like disruptions of associating-polymer solutions, *Phys. Rev. E* 51 (1995) 1338–1343.
- [8] O. Greffier, A. Al Kahwaji, J. Rouch, H. Kellay, Observation of a finite-time singularity in needle propagation in Hele–Shaw cells, *Phys. Rev. Lett.* 81 (1998) 3860–3863.
- [9] S. Koch, T. Schneider, W. Küter, The velocity field of dilute cationic surfactant solutions in a Couette-viscometer, *J. Non-Newtonian Fluid Mech.* 78 (1998) 47–59.
- [10] C.H. Liu, D.J. Pine, Shear-induced gelation and fracture in micellar solutions, *Phys. Rev. Lett.* 77 (1996) 2121–2124.
- [11] E.K. Wheeler, P. Fischer, G.G. Fuller, Time-periodic flow induced structures and instabilities in a viscoelastic surfactant solution, *J. Non-Newtonian Fluid Mech.* 75 (1998) 193–208.
- [12] P. Fischer, Time dependent flow in equimolar micellar solutions: transient behavior of the shear stress and first normal stress difference in shear induced structures coupled with flow instabilities, *Rheol. Acta* 39 (2000) 234–240.
- [13] A. Belmonte, Self-oscillations of a cusped bubble rising through a micellar fluid, *Rheol. Acta* 39 (2000) 554–559.

- [14] A. Jayaraman, A. Belmonte, Oscillations of a solid sphere falling through a wormlike micellar fluid, *Phys. Rev. E* 67 (2003) 65301–65304.
- [15] H. Rehage, H. Hoffmann, Shear induced phase transitions in highly dilute aqueous detergent solutions, *Rheol. Acta* 21 (1982) 561–563.
- [16] M.E. Cates, S.J. Candau, Statics and dynamics of wormlike surfactant micelles, *J. Phys.: Condens. Matter* 2 (1990) 6869–6892.
- [17] J.F. Berret, D.C. Roux, G. Porte, Isotropic-to-nematic transition in wormlike micelles under shear, *J. Phys. II* 4 (1994) 1261–1279.
- [18] P. Boltenhagen, Y. Hu, E.F. Matthys, D.J. Pine, Inhomogeneous structure formation and shear-thickening in worm-like micellar solutions, *Europhys. Lett.* 38 (1997) 389–394.
- [19] J. Eggers, Nonlinear dynamics and breakup of free-surface flows, *Rev. Modern Phys.* 69 (1997) 865–929.
- [20] X.D. Shi, M.P. Brenner, S.R. Nagel, A cascade of structure in a drop falling from a faucet, *Science* 265 (1994) 219–222.
- [21] D.M. Henderson, W.G. Pritchard, L.B. Smolka, On the pinch-off of a pendant drop of viscous fluid, *Phys. Fluids* 9 (1997) 3188–3200.
- [22] D.M. Henderson, H. Segur, L.B. Smolka, M. Wadati, The motion of a falling liquid filament, *Phys. Fluids* 13 (2000) 550–565.
- [23] P. Markovich, M. Renardy, A finite difference study of the stretching and break-up of filaments of polymer solutions, *J. Non-Newtonian Fluid Mech.* 17 (1985) 13–22.
- [24] M. Goldin, J. Yerushalmi, R. Pfeffer, R. Shinnar, Breakup of a laminar capillary jet of a viscoelastic fluid, *J. Fluid Mech.* 38 (1969) 689–711.
- [25] Y. Christanti, L.M. Walker, Surface tension driven break-up of strain-hardening polymer solutions, *J. Non-Newtonian Fluid Mech.* 100 (2001) 9–26.
- [26] M.D. Chilcott, J.M. Rallison, Creeping flow of dilute polymer solutions past cylinders and spheres, *J. Non-Newtonian Fluid Mech.* 29 (1988) 381–432.
- [27] T. Shikata, H. Hirata, T. Kotaka, Micelle formation of detergent molecules in aqueous media: viscoelastic properties of aqueous cetyltrimethylammonium bromide solutions, *Langmuir* 3 (1987) 1081–1086.
- [28] H. Rehage, H. Hoffmann, Viscoelastic surfactant solutions—model systems for rheological research, *Mol. Phys.* 74 (1991) 933–973.
- [29] C. Grand, J. Arrault, M.E. Cates, Slow transients and metastability in wormlike micelle rheology, *J. Phys. II* 7 (1997) 1071–1086.
- [30] T. Shikata, Y. Sakaiguchi, H. Uragami, A. Tamura, H. Hirata, Enormously elongated cationic surfactant micelle formed in CTAB aromatic additive systems, *J. Colloid Interface Sci.* 119 (1987) 291–293.
- [31] S.L. Keller, P. Boltenhagen, D.J. Pine, J.A. Zasadzinski, Direct observation of shear-induced structures in wormlike micellar solutions by freeze-fracture electron microscopy, *Phys. Rev. Lett.* 80 (1998) 2725–2728.
- [32] I.A. Kadoma, C. Ylitalo, J.W. van Egmond, Structural transitions in wormlike micelles, *Rheol. Acta* 36 (1997) 1–12.
- [33] S. Kumar, R.G. Larson, Shear banding and secondary flow in viscoelastic fluids between a cone and plate, *J. Non-Newtonian Fluid Mech.* 95 (2000) 295–314.
- [34] J.-Y. Lee, J.J. Magda, H. Hu, R.G. Larson, Cone angle effects, radial pressure profile, and second normal stress difference for shear-thickening wormlike micelles, *J. Rheol.* 46 (2002) 195–208.
- [35] J.-F. Berret, J. Appell, G. Porte, Linear rheology of entangled wormlike micelles, *Langmuir* 9 (1993) 2851–2854.
- [36] R.K. Prud’homme, G.G. Warr, Elongational flow of solutions of rodlike micelles, *Langmuir* 10 (1994) 3419–3426.
- [37] L.M. Walker, P. Moldenaers, J.-F. Berret, Macroscopic response of wormlike micelles to elongational flow, *Langmuir* 12 (1996) 6309–6314.
- [38] P. Fischer, G.G. Fuller, Z. Lin, Branched viscoelastic surfactant solutions and their response to elongational flow, *Rheol. Acta* 36 (1997) 632–638.
- [39] G.V. Vinogradov, A.Y. Malkin, V.V. Volosevitch, V.P. Shatalov, V.P. Yudin, Flow, high-elastic (recoverable) deformation, and rupture of uncured high molecular weight linear polymers in uniaxial extension, *J. Polym. Sci. Polym. Phys.* 13 (1975) 1721–1735.
- [40] W.M. Jones, I.J. Rees, The stringiness of dilute polymer solutions, *J. Non-Newtonian Fluid Mech.* 11 (1982) 257–268.
- [41] A.Y. Malkin, C.J.S. Petrie, Some conditions for rupture of polymer liquids in extension, *J. Rheol.* 41 (1997) 1–25.
- [42] R.J. Donnelly, W. Glaberson, Experiment on capillary instability of a liquid jet, *Proc. R. Soc. Lond. A* 290 (1966) 547–556.
- [43] W.S. Rayleigh, On the instability of jets, *Proc. Lond. Math. Soc.* 10 (1878) 4–13.

- [44] S. Tomotika, On the instability of cylindrical thread of a viscous liquid surrounded by another viscous liquid, *Proc. R. Soc. Lond. A* 150 (1935) 322–337.
- [45] B.J. Meister, G.F. Scheele, Generalized solution of the Tomotika stability analysis for a cylindrical jet, *AIChE* 13 (1967) 682–688.
- [46] Q. Wang, M.G. Forest, S.E. Bechtel, Modeling and computation of the onset of failure in polymeric liquid filaments, *J. Non-Newtonian Fluid Mech.* 58 (1995) 97–129.
- [47] G.H. McKinley, A decade of filament stretching rheometry, in: D.M. Binding, N.E. Hudson, J. Mewis, J.-M. Piau, C.J.S. Petrie, P. Townsend, M.H. Wagner, K. Walters (Eds.), *Proceedings of the XIIIth International Congress on Rheology*, vol. 1, British Society of Rheology, Cambridge, UK, 2000, pp. 15–22.
- [48] R.G. Larson, Instabilities in viscoelastic flows, *Rheol. Acta* 31 (1992) 213–263.
- [49] C. Venet, B. Vergnes, Experimental characterization of sharkskin in polyethylenes, *J. Rheol.* 41 (1997) 873–892.
- [50] L.B. Smolka, A. Belmonte, Effects of salt on filament dynamics during drop pinch-off in xanthan gum solutions, *Phys. Fluids*, 2000, submitted for publication.
- [51] W.M. Jones, N.E. Hudson, J. Ferguson, The extensional properties of M1 obtained from the stretching of a filament by a falling drop, *J. Non-Newtonian Fluid Mech.* 35 (1990) 263–276.
- [52] R.G. Larson, *Constitutive Equations for Polymer Melts and Solutions*, Butterworths, Boston, 1988.
- [53] J.M. Rallison, E.J. Hinch, Do we understand the physics in the constitutive equation? *J. Non-Newtonian Fluid Mech.* 29 (1988) 37–55.